ACS Sustainable Chem. Eng. 2017, 5, 4, 3087–3095

High-Performance Magnetic Activated Carbon from Solid Waste from Lignin Conversion Processes. 1. Their Use As Adsorbents for CO

*Wenming Hao[a,b], Fredrik Björnerbäck[a,b], Yulia Trushkina[a], Mikel Oregui Bengoechea[c], German Salazar-Alvarez[a], Tanja Barth[c], Niklas Hedin,[a,b]**

[a] *Department of Materials and Environmental Chemistry, Arrhenius Laboratory, Stockholm University, SE-106 91 Stockholm, Sweden*

[b] *Berzelii Center EXSELENT on Porous Materials, Arrhenius Laboratory, Stockholm University, SE-106 91 Stockholm, Sweden*

[b] *Department of Chemistry, University of Bergen, N-5007 Bergen, Norway*

Keywords: CCS, magnetic activated carbon, lignin conversion, hydrochar, separation, adsorption, desorption

DOI: https://doi.org/10.1021/acssuschemeng.6b02795

Abstract

Lignin is naturally abundant and a renewable precursor with the potential to be used in the production of both chemicals and materials. As many lignin conversion processes suffer from a significant production of solid wastes in the form of hydrochars, this study focused on transforming hydrochars into magnetic activated carbons (MAC). The hydrochars were produced via hydrothermal treatment of lignins together with formic acid. The activation of the hydrochars was performed chemically with KOH with a focus on the optimization of the MACs as adsorbents for CO_2. MACs are potentially relevant to carbon capture and storage (CCS) and gas purification processes. In general, the MACs had high specific surface areas (up to 2875 m^2/g), high specific pore volumes, and CO_2 adsorption capacities of up to 6.0 mmol/g (1 atm, 0 °C). The textual properties of the MACs depended on the temperature of the activation. MACs activated at a temperature of 700 °C had very high ultramicropore volumes, which are relevant for potential adsorption-driven separation of CO_2 from N_2. Activation at 800 °C led to MACs with larger pores and very high specific surface areas. This temperature-dependent optimization option, combined with the magnetic properties, provided numerous potential applications of the MACs besides those of CCS. The hydrochar was derived from eucalyptus lignin, and the corresponding MACs displayed soft magnetic behavior with coercivities of <100 Oe and saturation magnetization values of 1–10 emu/g.

Introduction

Fossil resources are being depleted[1] and their use is associated with emissions of greenhouse gases which contribute to anthropogenic global warming.[2] As production of materials is significantly interlinked with the use of fossil resources, developing materials from renewable resources can reduce the emissions of greenhouse gases.

An underused source of renewable materials and chemicals is the amorphous and largely aromatic polymer lignin.[3–6] Lignin is a major component in wood and about 50 million tons are produced annually.[7] It is generally considered a waste product with a low added value. Today about 98% of the available lignin is combusted to supply the pulping and paper processes with energy and low-grade heat.

Most of the remaining lignin is used for deriving low-value products or in narrow market segments.[7] However, the potential of lignin to be used as a precursor in the production of renewable chemicals and materials is high, and consequently, it is researched for future use in biorefineries[3,4] and materials production. The structure and chemistry of lignin, as well as the approaches to lignin depolymerization/ repolymerization, depend on the type of wood it originates from and the processes used for its separation.[8] Attempts to produce liquid fuels and chemicals from lignin have often suffered from large streams of side-products consisting of solid wastes[5,6,9]. By transforming such solid wastes into functional materials, it could be possible to simultaneously add commercial value to the lignin and reduce its associated ecological footprint. The solid wastes have, e.g., the potential to be used as precursors for renewable and functional materials such as activated carbons (ACs).

ACs are highly porous materials commonly used in industry for catalysis, purification, decolorization, deodorization, and resources,[11,12] but wood and coconut shells are also important precursors.[13] The use of lignin directly for the production of ACs has been studied.[14–19] In 2014, the production of ACs was estimated at 1.4 million tons,20 and the market value is expected to continue to increase from $2.1 billion in 2014 with a compound annual growth rate at above 10% in the upcoming years.[21] The increase is in part a result of stricter regulations on mercury emissions from industry and various aqueous contaminants.[21,22]

ACs may find use as CO_2 adsorbents in carbon capture and storage (CCS) because of their potential to reduce the cost for capture of CO_2, which is a major hurdle for the implementation of CCS systems.[23–27] ACs have the advantages of high adsorption capacity, low cost, and outstanding cycling performance as compared to most other adsorbents.[26] However, for the CO_2 adsorption processes to be viable, the cycling times need to be fast; i.e., the adsorption and desorption should be fast.[28] For adsorption processes in the liquid state, powdered activated carbons (PACs) are generally more effective than granular activated carbons (GACs), due to their smaller particle size. However, the small particle size also makes the separation of PACs from liquids much more difficult than the separation

of GACs.[29]

Magnetic activated carbons (MACs) may allow for new use of ACs in various processes. MACs and other porous materials with magnetic properties have previously been produced.[30–33] Chemical coprecipitation[31,34–37] with paramagnetic or ferromagnetic compounds is a promising approach. Ball milling38 and impregnation[39,40] can also be used to introduce such compounds with magnetic properties into the ACs. Suspended powdered MACs may be separated from liquids with a use of an external magnetic field.[31,32] In this study, solid byproducts from the conversion of lignin into biooil[6,9] were used to produce MACs with magnetic properties originating from iron-containing nanoparticles. The MACs could be optimized to either contain very high large ultramicropore volumes or present very large surface areas.

Experimental section

Materials

All reagents were of high purity grade and used as supplied, unless otherwise stated.

Lignin conversion to biooil and hydrochars

The hydrochars were produced as side products from a lignin-to-liquid process performed under hydrothermal conditions together with formic acid, as has been described elsewhere.[9] Two different types of lignin were used for the production of hydrochars. The eucalyptus lignin originated from Thailand and was processed in a biorefinery demonstration plant of SEKAB in Örnsköldsvik, Sweden, using enzymatic hydrolysis. The lignin from Norway spruce was produced at Processum (Sweden) by acid precipitation from kraft black liquor supplied by the Metsä Board Husum mill in Sweden. The elemental analysis of lignin is presented in Table S1. In a typical batch used for the production of a hydrochar, first, 200 g of lignin, 200 mL of formic acid, 500 g of water, and the catalyst were added to a 5 L stainless-steel reactor. The closed reactor was subsequently heated to the desired temperature for 2 h. A temperature of 380 °C was used to produce hydrochars from the Kraft lignin from Norway spruce and 365 °C when using the lignin derived by enzymatic hydrolysis of eucalyptus biomass. After cooling the reactor down by natural convection, the hydrochars were separated and dried. The hydrochars prepared from lignin from Eucalyptus and Spruce, having yields of 29.63% and 33.42%, are called HC-E and HC-S, respectively.

Activation of hydrochars into magnetic activated carbons

HC-E and HC-S were chemically activated into ACs by KOH batchwise. Three grams of HC-E or HC-S was combined with 30 mL of an aqueous solution of KOH (six mol/dm^3) and treated overnight at room temperature. The mixtures were heated for 5 h at a temperature of 200 °C and subsequently activated under a flow of N_2 (48 dm^3/h) for 4 h at a temperature of 700 or 800 °C. During the activation, the temperature was increased to the set point at a rate of 10 °C/min. After being cooled down by natural convection, the powders were washed with hot water until the pH of the effluents

reached neutral values. The corresponding samples were dried at a temperature of 110 °C for 12 h. The set of samples are denoted as MAC-E-X or MAC-S-X. E and S stand for a lignin source of Eucalyptus and Spruce, respectively; X (7 or 8) is the temperature of the activation (700 or 800 °C).

Elemental analysis

CHN analyzes were conducted by using combustion analysis. The amounts of Fe were analyzed by a Varian Vista MPX ICP-OES system. The amounts of O were calculated by difference (the samples were assumed to be composed of only C, H, N, Fe and O).

Adsorption measurements

Adsorption isotherms for N_2 were measured at -196 ºC using a Micromeritics ASAP 2020 device. Before experimentation, samples were degassed under conditions of dynamic vacuum at a temperature of 300 ºC for 5 h.

Specific surface areas (S_{BET}) were calculated in the Brunauer–Emmet–Teller (BET) model, using the uptake of N_2 at relative pressures (p/p_0) between 0.06 and 0.29. Care was taken to assure positive and not unphysically large c-values by adjusting the exact pressure range. The total pore volume (V_t) was estimated from the uptake at $p/p_0 = 0.99$. The external surface area (S_{ext}) and micropore volumes (V_{mic}) were determined with the t-plot method. The micropore surface area (S_{mic}) was determined as the difference between the S_{BET} and S_{ext}. The pore-size distributions were estimated from the N_2 adsorption branch using a density functional theory (DFT) method supplied by Micromeritics.

The adsorption and desorption of CO_2 on the MACs were measured with the same Micromeritics device at temperatures of 0, 20, 50, and 80 ºC, which were controlled by a circulating bath. The pressure used was from 0 to 101 kPa. Samples were degassed under the condition of a dynamic vacuum at a temperature of 300 ºC for five hours before conducting the measurements. Ultramicropore volumes were determined from the adsorption data of CO_2 at 0 ºC, with the Dubinin-Radushkevich (DR) method.

Scanning electron microscopy

The scanning electron microscopy (SEM) images were captured with a JEOL JSM-7000F microscope using a working distance of 10 mm and an accelerating voltage of 5.0 kV. Detection of secondary electrons was used. Samples were fixed on Oxford Aluminum stubs and coated by dried colloidal carbon before SEM analyses.

Transmission electron microscopy

Transmission electron microscopy (TEM) images were used to determine sample morphology and distribution of iron-based particles in the carbon matrix. The specimens were prepared by depositing a drop of a dilute ethanol suspension of the powders on carbon-coated copper grids (TedPella) and letting the solvent evaporate under atmospheric conditions. Bright field images were collected with either a JEM-2100 (JEOL) microscope (LaB6 filament, 200 kV, f = 2.7 mm, Cs = 1.4 mm, Cc = 1.8 mm, point resolution = 2.5 Å, lattice resolution = 1.4 Å) equipped with a Gatan SC1000 ORIUS camera or a JEM-2100F (JEOL) microscope with a Schottky-type field emission gun working at 200 kV (f = 1.9 mm, Cs = 0.5 mm, Cc = 1.1 mm, point resolution =1.9 Å, lattice resolution =1.0 Å) equipped with a Gatan Ultrascan 1000 camera.

Powder X-Ray diffraction

The powder was glued with silicon grease onto a thin glass fiber, and powder X-ray diffraction (PXRD) patterns were collected in transmission mode with a dark current mode with Xcalibur III Single Crystal diffractometer (Mo Kα radiation with λ = 0.709317 Å), equipped with a two-dimensional Sapphire 3 CCD detector (2048 × 2048 px^2 and pixel size = 30 × 30 μm^2). Data were averaged over four scans, each with a 2θ range of 0−49° (d = 6.97−0.85 Å), exposure time of 2400 s, and a sample-to-detector distance of 120 mm. The instrumental width was determined through the calibration of the peak width of a lanthanum hexaboride (LaB_6) powder, which was measured using the same procedure.

Magnetic measurements

Magnetic measurements were performed at room temperature with a LakeShore VSM 7400 vibrating sample magnetometer using a pole gap of 22 mm. The field-dependent magnetization curves were measured between ±18 kOe. The specimens were fixated in gelatin capsules and sealing varnish whereas the magnetization scale was calibrated with a Ni sphere.

Results and discussions

The precursors (HC-E and HC-S) had C−H−N−O compositions typical for hydrochars produced in lignin-to-liquid biofuel processes operating under hydrothermal conditions at temperatures of 365−380 °C and with formic acid present.9 The detailed compositions are shown in Table 1.

Iron had been introduced into both HC-E and HC-S, which could have been introduced from both the corrosion of the stainless steel reactor and by the lignin. As shown in Table S1, the lignin consists of a certain amount of iron. Corrosion is often judged as one of the limiting factors of hydrothermal liquefaction of biomass.41 Eventhough we did not observe any significant corrosion on the surface of the stainless steel reactor, it strongly indicates that a part of the iron was included from corrosion. Moreover, the presence of iron is likely to have promoted the graphitization of carbon, as shown in the XRD result in Figure 1, which resulted in some bamboo-like structures such as those shown in Figure 2d.42 However, here, the introduction of iron into the hydrochars was serendipitous and rendered both the precursors and related MACs magnetic. The HC-S had an Fe content of 12.3 wt % and could easily be attracted to a magnetic field, while the HCE had an Fe content of 2.94 wt %. The carbon and iron content in the MAC-E series increased upon activation, but both the C and Fe content decreased upon activation of the MAC-S-8, which possibly was related to the large ash content of HC-S, see Table 1 and Figures S2−S4. The MACs contained large amounts of ash (Table 1 and Figures S2−S4) that could be partially dissolved by treatment with base and acid solutions (see Figure S5).

Table 1. Ash content, bulk element composition of the precursor and the activated carbon

Sample	Ash[a] (wt.%)	Ultimate (wt.%)				
		C	H	N	Fe	others
HC-S	31.6	59.20	3.14	<0.10	12.29	25.27
HC-E	16.4	69.02	3.68	0.64	2.94	23.72
MAC-S-8	19.6	49.56	0.88	0.30	7.10	42.16
MAC-E-7	19.8	72.19	0.91	0.47	4.71	21.72
MAC-E-8	27.2	75.97	0.90	0.39	6.40	16.34

[a] Determined by thermal gravimetry conducted in air at 800 °C, *c.f.* Figure S1-3. HC-E is a hydrochar from lignin of Eucalyptus; HC-S is a hydrochar from lignin of spruce; MAC-E-X and MAC-S-X are magnetic activated carbons prepared from HC-E and HC-S; X (7 or 8) is the temperature of the activation (700 °C or 800 °C).

Morphology and structure of the magnetic activated carbons

In the SEM images, the two hydrochars appeared as contiguous pieces of matter, see Figure 3a (HC-E) and Figure 3b (HC-S); however, after the KOH-based chemical activation, the morphologies of the samples changed. The SEM images of the corresponding MACs displayed cavities at the micromolarlength scale, see Figure 3c−f. The MACs that had been KOH-activated at a temperature of 700 °C (MAC-E-7 in Figure 3c and MAC-S-7 in Figure 3d) contained smaller cavities than those activated at 800 °C (MAC-E-8 in Figure 3e and MAC-S-8 in Figure 3f). The chemical activation with KOH appears to have created these etched cavities.

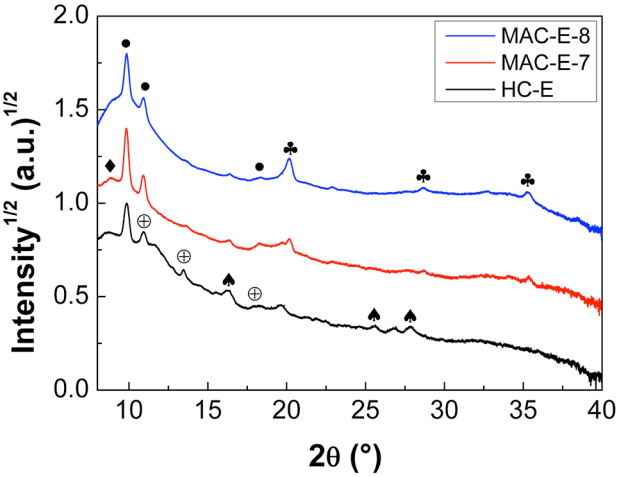

Figure 1. Powder X-ray diffraction (Mo Kα) patterns of the Eucalyptus precursor and activated samples. The symbols represent the peak position for some of the most intense peaks of graphite oxide (♦), magnetite (♠), metallic iron (♣), iron sulfate - jarosite (⊕), and sample holder (●). HC-E is the hydrochar from the Eucalyptus lignin; MAC-E-X's are corresponding magnetic activated carbons prepared at a temperature of 700 or 800 °C.

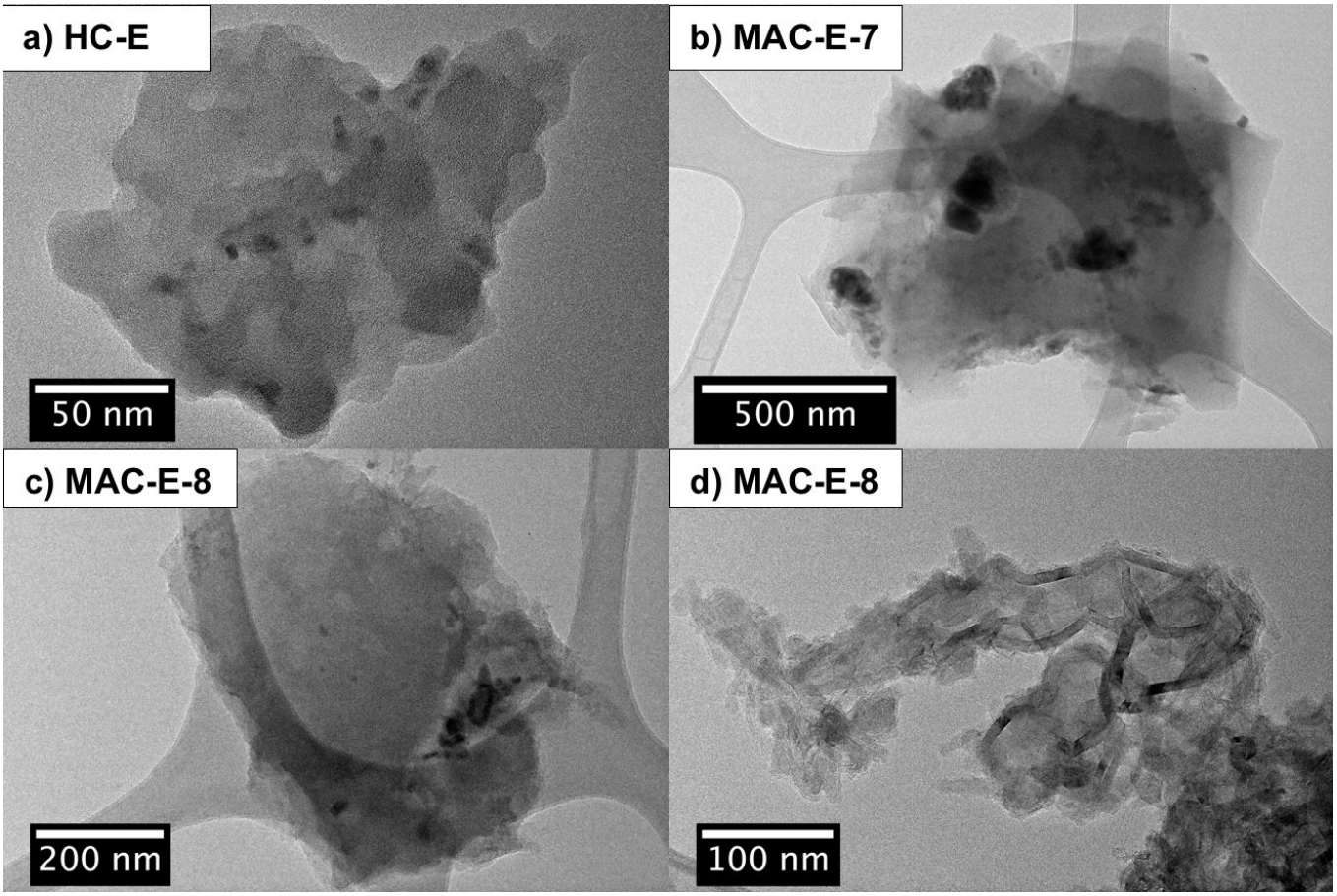

Figure 2. Bright-field transmission electron microscopy images of (a) the precursor HC-E and (b-d) the activated samples. The dark spots in a-d correspond to iron-containing particles on a carbon matrix whereas the long fibers in d correspond to graphitic structures. HC-E is hydrochar from the Eucalyptus lignin; MAC-E-Xs are corresponding magnetic activated carbons prepared at temperature of 700 or 800 °C.

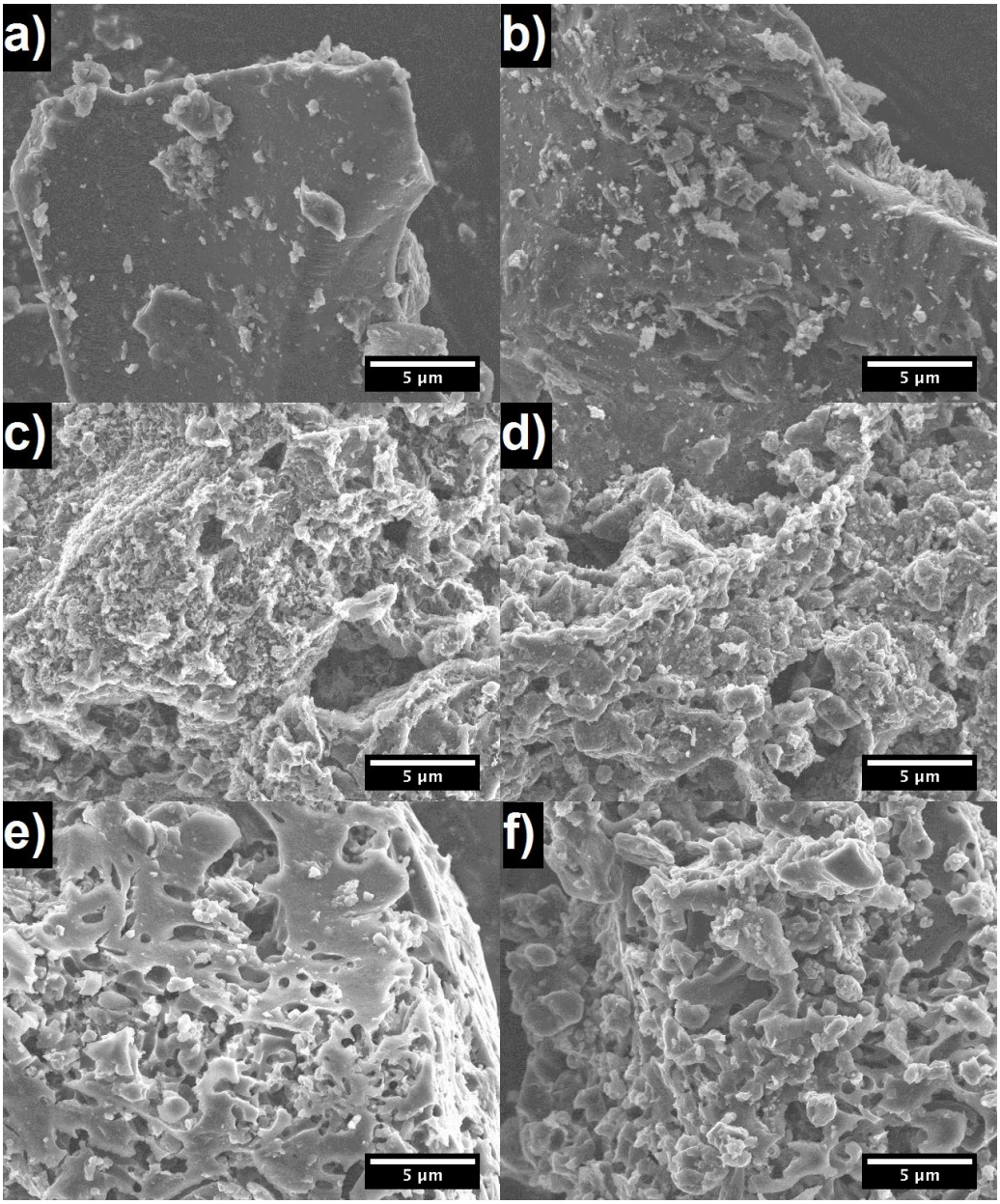

Figure 3. Scanning electron microscopy (SEM) images of a) HC-E, b) HC-S, c) MAC-E-7, d) MAC-S-7, e) MAC-E-8, f) MAC-S-8. HC-E is hydrochar from the Eucalyptus lignin; HC-S is hydrochar from spruce lignin; MAC-E-X and MAC-S-X are magnetic activated carbons prepared from HC-E and HC-S, X (7 or 8) is the temperature of the activation (700 °C or 800 °C).

In addition to the morphological variations visible in the SEM images of the hydrochars and the MACs, the chemically activated MACs were highly porous in the microporous (<2 nm) and/or mesoporous (2−50 nm) domains. The terms microporous and mesoporous are used in accordance with the definitions of IUPAC.[43] The N_2 adsorption and desorption isotherms in Figure 4a showed that MAC-S-7 and MAC-E-7 had the typical characteristics of microporous materials. The adsorbed amount of N_2 increased sharply on raising the N_2 gas pressure at low pressures, and the adsorbed amount leveled out at a distinct plateau at higher pressures. MAC-E-7 had smaller pores than MAC-S-7, as can be seen in the pore size distributions (PSDs) of Figure 4b.

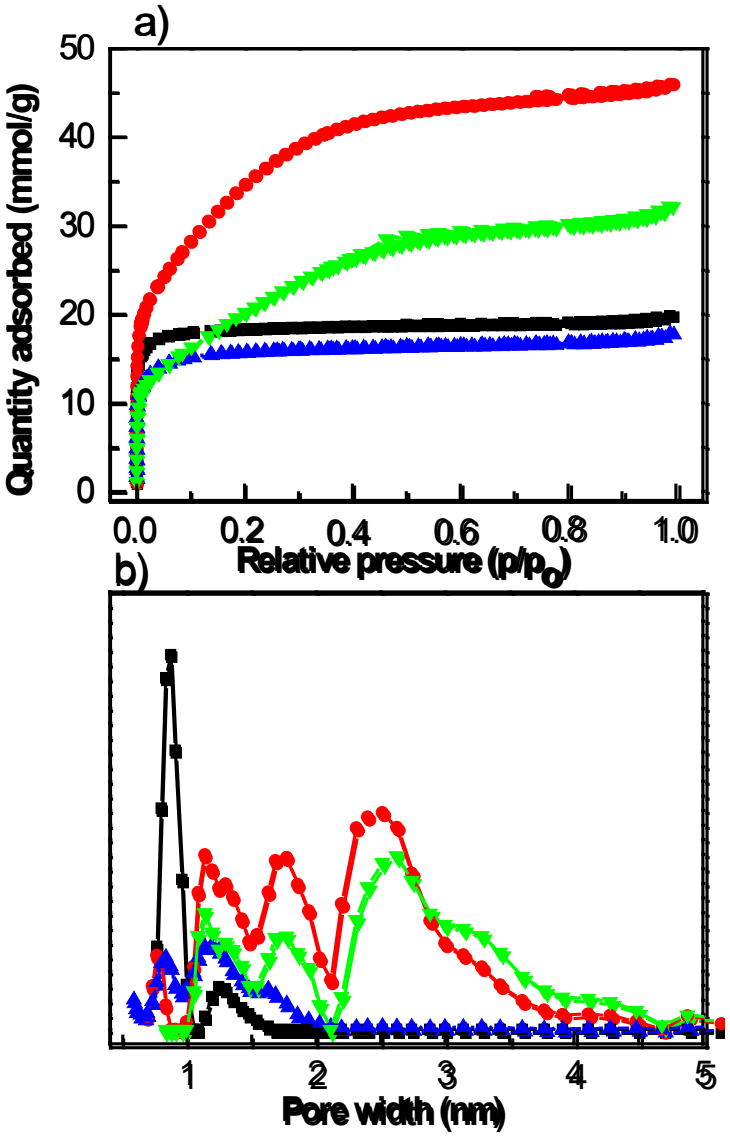

Figure 4. N_2-adsorption and desorption isotherms (a) at -196 °C and pore size distributions (b, using DFT model) of magnetic activated carbons from hydrochars: MAC-E-7, "■ (black)"; MAC-S-8, "▼ (green)"; MAC-E-8, "● (red)"; MAC-S-7, "▲ (blue)". MAC-E-X and MAC-S-X are magnetic activated carbons prepared from hydrothermally treated Eucalyptus lignin (E) and spruce lignin (S), X (7 or 8) is the temperature of the activation (700 °C or 800 °C).

MAC-E-8 and MAC-S-8 contained significant fractions of mesopores with sizes between 2 and 4 nm, in addition to the micropores as displayed in the PSDs of Figure 4b. Similar relations between a high activation temperature and the formed mesopores have been identified by others.[44,45] As was expected, MAC-X-8 had a higher surface area (S_{BET}) and external surface area (S_{ext}) and a larger pore volume than MAC-X-7, but its micropore volume (V_{mic}) was smaller. In particular, MAC-E-8 had a BET surface area of 2875 m^2/g and a pore volume of 1.59 cm^3/g, which are among the highest observed for ACs prepared from hydrochars. Textural characteristics were derived from the N_2-adsorption and desorption isotherms and are shown in Table 2. By alternating treatment with NaOH and HCl solutions, the S_{BET} of MAC-E-7 increased from 1650 m^2/g to 1760 m^2/g, as is presented in Table S2, and the corresponding isotherms are shown Figure S6. Ding et al. prepared an AC from hydrothermally treated rice husks by chemical activation with KOH, which had a S_{BET} of 3322 m^2/g and a V_{tot} of 2.53 cm^3/g.[46] Sevilla et al. also reported on a KOH-activated AC from hydrothermally carbonized sawdust with a S_{BET} of 2850 m^2/g and a V_{tot} of 1.35 cm^3/g.[47] Similarly, Wei et al. prepared an AC from hydrothermally carbonized wood by KOH activation with a S_{BET} of 2970 m^2/g and V_{tot} of 1.35 cm^3/g.[48] The S_{ext} was very high (2580 m^2/g), and its V_{mic} was small (0.07 cm^3/g).

Table 2. Yield, textural properties, uptake of CO_2 and apparent selectivity of magnetic activated carbons from hydrochar

MAC[c]	Yield (%)	CO_2 uptake (0 °C, 101 kPa) (n, mmol/g)	CO_2 uptake (0 °C, 15 kPa) (n, mmol/g)	Apparent selectivity (CO_2/N_2)[a]	Specific surface area (m^2/g)			Specific pore volume (cm^3/g)		
					S_{BET}	S_{mic}	S_{ext}	V_t	V_{mic}	V_{utmic}[b]
MAC-E-7	51	6.0	1.8	15	1647	1571	76	0.69	0.60	0.38
MAC-E-8	37	3.7	0.9	16	2875	293	2582	1.59	0.07	0.12
MAC-S-7	78	3.8	1.1	11	1380	1156	224	0.62	0.45	0.24
MAC-S-8	39	2.1	0.5	11	1706	116	1590	1.12	0.02	0.10

[a] Apparent selectivity defined as $s= (n_{CO2}/n_{N2}) / (P_{CO2}/P_{N2})$, n is the uptake of CO_2 and N_2, P is the partial pressure of CO_2 (15 kPa) and N_2 (85 kPa).

[b] Ultramicropore volume determined by CO_2 adsorption at 0 °C with the DR method.

[c] MAC-E-X and MAC-S-X are magnetic activated carbons prepared from hydrothermally treated Eucalyptus lignin (E) and spruce lignin (S), X (7 or 8) is the temperature of the activation (700 °C or 800 °C).

As expected, chemical activation at a temperature of 700 °C gave higher yields than at 800 °C. MAC-S-7 had a very high yield (78%), which is consistent with that chemical activation usually has a higher yield than physical activation.[49,50] With activation at 800 °C, the MACs had larger pore volumes and higher surface areas, see Table 2. This temperature dependence is consistent with the findings of Otowa et al.[51]

Local structure, composition, and magnetism

Both the HC-E and the MAC-E's consisted of micrometer-sized carbon flakes with embedded iron-based particles of various sizes, which can be seen in the TEM images of Figure 2. For HC-E, the carbon flakes were amorphous. This sample contained iron-based particles with crystallites <10 nm. For MAC-E-7/8, the carbon flakes were more faceted, indicating a higher crystallinity of the carbon network (c.f. Figure 1). The iron-based particles were much larger in the MAC-E-7/8 than in the HC-E with sizes of 10− 100 nm.

The XRD pattern of HC-E in Figure 1 indicates that the iron-based particles consisted mainly of iron oxide (magnetite, Fe_3O_4) but also of iron hydroxysulfate (jarosite, $AFe_3(OH)_6(SO_4)_2$; A = H+, Na+, K+). The carbon was mainly amorphous with a small amount of graphite oxide. The activated sample AC-E-7 contained amorphous carbon, graphite oxide, and metallic α-Fe with a passivation layer consisting of magnetite. The activated sample AC-E-8 contained a larger amount of α-Fe (with its passivation layer) and a larger amount of graphitized carbon than AC-E-7. The broad signal of the graphitized carbon was masked by the peaks from the sample holder.

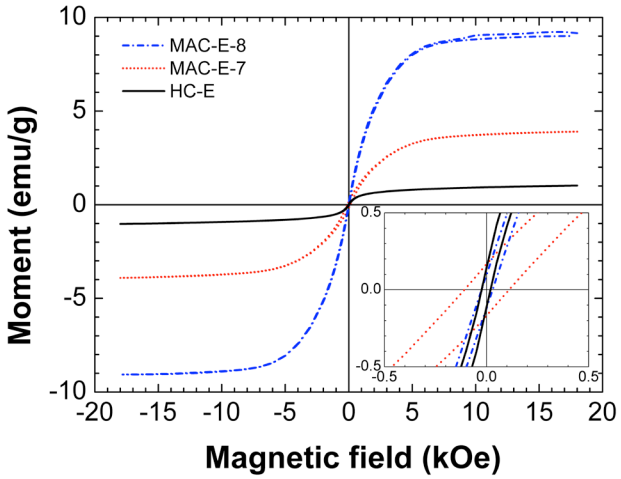

Figure 5. Magnetic measurements of the hydrochar and the activated carbons. Magnetization vs field hysteresis curves with máximum applied field Hmax = 18 kOe. HC-E is the hydrochar from the Eucalyptus lignin; MAC-E-X's are corresponding magnetic activated carbons prepared at a temperature of 700 or 800 °C.

The magnetization curves of HC-E and the MAC-Es are shown in Figure 5 and showed soft magnetic behavior with coercivities below 100 Oe. The saturation magnetization values were 1.1, 4.1, and 9.5 emu/g for HC-E, AC-E-7, and AC-E-8, respectively, and depended on the iron content of the samples and the composition of the iron compounds. For instance, the saturation magnetization of α-Fe is ~210 emu/g, but that of magnetite is ~90 emu/g. Hence, the activated samples AC-E-7 and AC-E-8 containing α-Fe had a larger saturation value than the hydrochar HC-E that contained Fe_3O_4.

Adsorption of CO_2 and N_2 at temperatures of 0 °C and above

The adsorption of CO_2 and N_2 on the MACs were studied at a common standard temperature of 0 °C[52,53] but also at the higher temperatures applicable to CO_2 capture. Flue gas has typically a temperature between 40 and 120 °C after heat exchange,[54] and the total pressure is close to atmospheric. The partial pressure of CO_2 is about 15 kPa for the flue gas from a coal-fired power plant and about 5 kPa for the one from a natural-gas fired one.[55]

At 0 °C, MAC-E-7 had an uptake of CO_2 of 6.0 mmol/g at 101 kPa and 1.8 mmol/g at 15 kPa (Figure 6) and increased to 6.2 mmol/g at 101 kPa and 1.9 mmol/g at 15 kPa after partial removal of ash (Figure S7 and Table S2). Similar values have been reported in the literature for ACs at this temperature. Alabadi et al. reported on a microporous AC, prepared from a mixture of starch and gelatin by KOH through dry chemical activation. The AC had an uptake of CO_2 of 7.5 mmol/g at 101 kPa.[53] Sevilla et al. synthesized a KOH-activated AC from hydrothermally treated sawdust with an uptake of CO_2 of 6.6 mmol/g at 101 kPa and 1.8 mmol/g at 15 kPa[47] and an N-doped AC from hydrothermally carbonized algae with an uptake of CO_2 of 7.4 mmol/g at 101 kPa.[56] Deng et al. reported on an AC derived from pine-nut shells with an uptake of CO_2 of 7.7 mmol/g at 101 kPa and 3.3 mmol/g at 15 kPa.[57] It has been reported that the subatmospheric adsorption of CO_2 at ambient temperatures is related to the (ultra)micropore volume.[27,49,56,57] MAC-E-7 had a smaller S_{BET} than MAC-E-8. MAC-E-7 had the highest ultramicropore and micropore volumes among the four MACs studied, see Table 2. The PSDs of the four MACs were also estimated using a DFT model and the CO_2 adsorption data recorded at 0 °C (Supporting Information Figure S8). Even though large pores do not contribute to the adsorption of CO_2 at pressures relevant to postcombustion capture of CO_2, such large pores might become important to the mass transport of CO_2. Montagnaro et al. showed that ACs with mesopores had a lower intraparticle diffusion resistance than ACs with mainly micropores.[58]

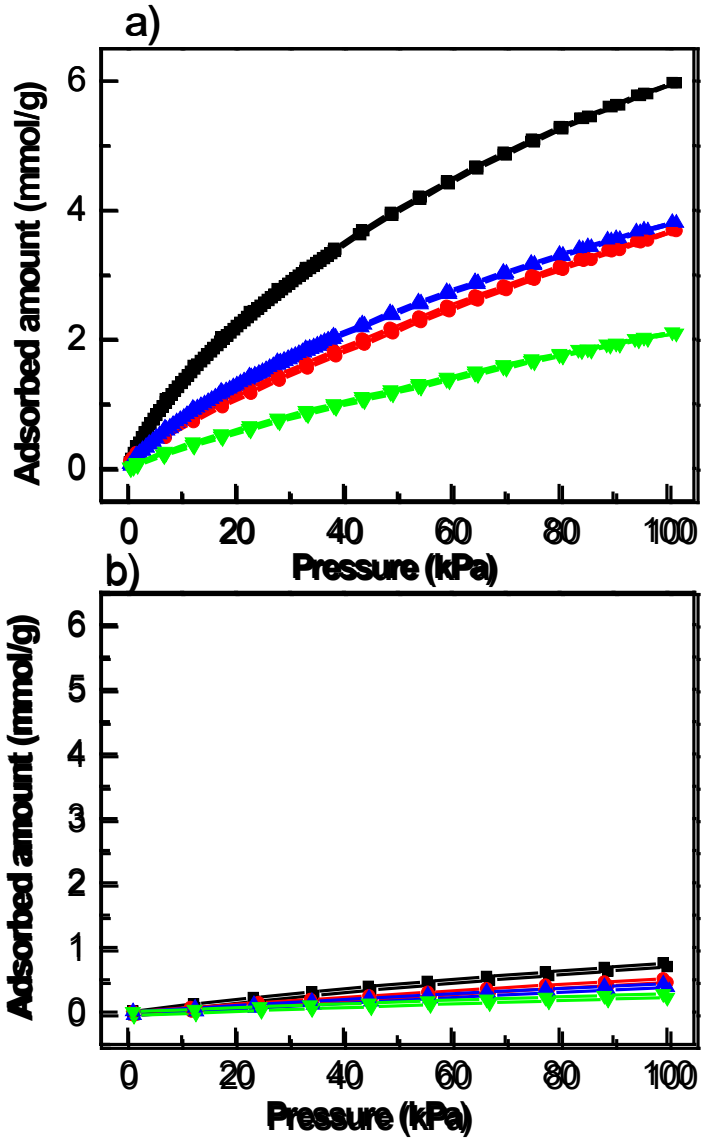

Figure 6. Adsorption and desorption isotherms of a) CO_2 and b) N_2 recorded at 273 K. Chemically activated carbons from hydrochars: MAC-E-7, "■ (black)"; MAC-S-8, "▼ (green)"; MAC-E-8, "● (red)"; MAC-S-7, "▲ (blue)". MAC-E-X and MAC-S-X are magnetic activated carbons prepared from hydrothermally treated Eucalyptus lignin (E) and spruce lignin (S), X (7 or 8) is the temperature of the activation (700 °C or 800 °C).

The CO_2-over-N_2 selectivity as well as the CO_2 capacity is key to CO_2 capture.56,59 As it is rather complex and timeconsuming to determine the binary selectivity experimentally, it is often estimated from single component adsorption data. There are numerous ways to estimate and express the selectivity, and here the apparent selectivity of CO_2/N_2 is often defined as $s = (n_{CO2}/n_{N2})/(P_{CO2}/P_{N2})$. n is the uptake of CO_2 and N_2; P is the partial pressure of CO_2 (15 kPa) and N_2 (85 kPa). For MAC-E-7, this selectivity was also estimated for a more realistic temperature of 50 °C. The selectivity was about 14 at a temperature of 50 °C (adsorption and desorption isotherms of N_2 and CO_2 are shown in the Supporting Information). The selectivity was somewhat reduced at the higher temperature, which is consistent with the study of Alabadi et al.[53] Overall, these estimated selectivity values are larger than those in the literature: Deng et al. reported a CO_2-over-N_2 selectivity of 8.4 at a temperature of 25 °C for the pinenut-shell-derived AC.[57] The ACs from hydrothermally carbonized algae prepared by Sevilla et al. have CO_2-over-N_2 selectivity of 10 at a temperature of 25 °C.[56]

The CO_2-over-N_2 selectivity of MAC-E-7 was also estimated by using the full ideal adsorption solution theory (IAST). The IAST was derived by Mayer and Prausnitz and uses single component adsorption data to predict adsorption equilibria of multicomponent mixtures.[60] The CO_2 and N_2 adsorption isotherms of MAC-E-7 at 0 and 50 °C were analyzed in the Toth model (see Figure S9 in the Supporting Information). These regression analyses were used as inputs to predict the binary CO2-over-N_2 selectivity for binary mixtures of CO_2 (15%)− N_2 (85%), using the IAST.[61,62] This selectivity estimate is presented by the molar uptake ratio of n(CO_2, binary)/n(N_2, binary) versus pressures, in Figure 7. The IAST-predicted selectivity was between 3 and 4 and notably lower than the simplified estimates presented above. The selectivity was lower at high than at low temperature. It also decreased as the pressure increased, which is contrary to the trends presented by Yi et al.[61] for another AC using the same IAST method.

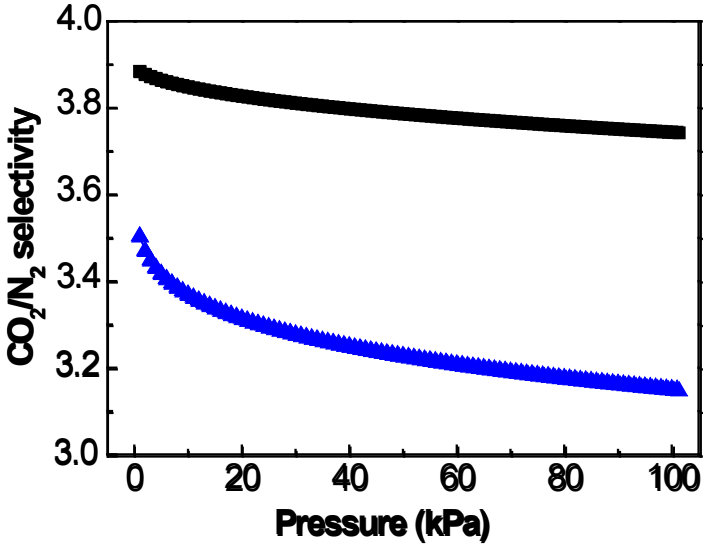

Figure 7. Selectivity of CO_2-over-N_2 under different pressures at temperatures of 0 °C, "■ (black)" and 50 °C, "▲ (blue)", for chemically activated carbon MAC-E-7 (activated at 700 °C from hydrothermally treated Eucalyptus), predicted by ideal adsorption solution theory.

Isosteric heat of CO_2 adsorption

The isosteric heat (Q_{st}) of CO_2 sorption is important for adsorption-driven capture of CO_2. If the Q_{st} is too large, the regeneration of the sorbents becomes too costly, and if it is too small, the CO_2 uptake and CO_2-over-N_2 selectivity will be too small.[63] It has been suggested that relevant values of Q_{st} are in the range of 30-70 kJ/mol for ACs with typical CO_2 concentrations in flue gas.[53,55,64– 66] As adsorption is an exothermic process, the amount of adsorbed CO_2 decreases with an increased temperature.[55,67]

The Q_{st} can be determined either calorimetrically,[68] or by using temperature and pressure dependent data and thermodynamic relations such as the van't Hoff,[69] or the Clapeyron-Clausius equation.[53,56,64,66,70] By the first and the last methods loading-dependent Q_{st} can be determined. From the adsorption and desorption isotherms in Figure 8a, the loading dependent Q_{st} for MAC-E-7 was calculated using the Clapeyron-Clausius equation: $Qst = R(\frac{\partial \ln P}{\partial T^{-1}})_n$.[63] Such corresponding isosters are

plotted in Figure 8b. The Q_{st} for MAC-E-7 was 27 - 30 kJ/mol at 50 °C, as is shown in Figure 8c. This level is somewhat lower than determined for related ACs prepared by activation in CO_2 in earlier work.[53,56,64-66]

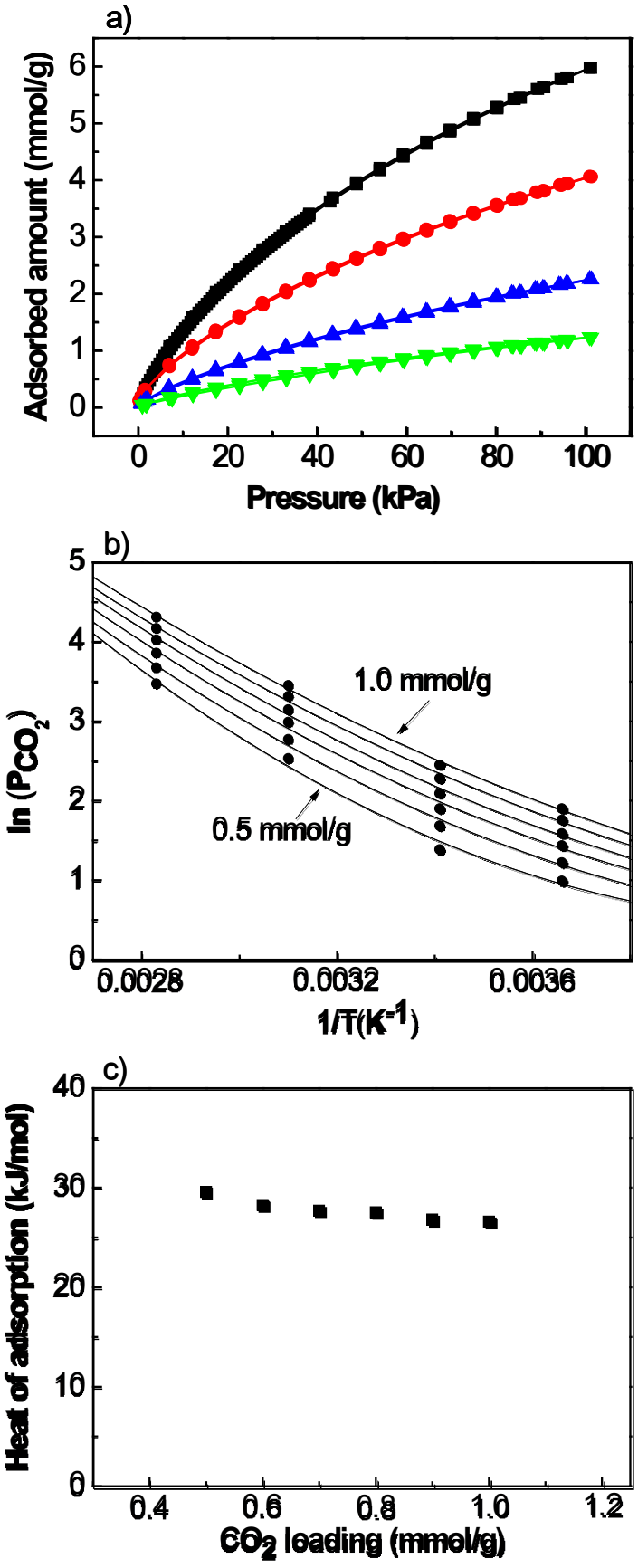
a)
Adsorbed amount (mmol/g)
Pressure (kPa)
b)
ln (PCO2)
1.0 mmol/g
0.5 mmol/g
1/T(K-1)
c)
Heat of adsorption (kJ/mol)
CO2 loading (mmol/g)

Figure 8. a) Adsorption and desorption isotherms of CO_2 at different temperatures for chemically activated carbon MAC-E-7 (activated at 700 °C from hydrothermally treated Eucalyptus) at 0 °C, "■ (black)"; 20 °C, "● (red)"; 50 °C, "▲ (blue)"; 80 °C, "▼ (green)". b) Plotted values of ln (P_{CO2}) versus 1/T for CO_2 on MAC-E-7 at constant loading of CO_2 (the contour lines are the regression analysis using a 2nd order polynomial). c) Heat of CO_2 adsorption (Q_{st}) as a function of CO_2 loading on MAC-E-7 at 50 °C. The Q_{st} values were calculated using the Clapeyron-Clausius equation.

Cycle performance and time dependent uptake of CO_2

As CO_2 adsorbents need to be reused many times the cyclic performance is important. Almost no noticeable drop was observed for MAC-E-7 after 9 cycles of repeated CO_2 adsorption and desorption, see Figure 9a. The cyclic CO_2 adsorption was determined without any heat regeneration between subsequent runs.

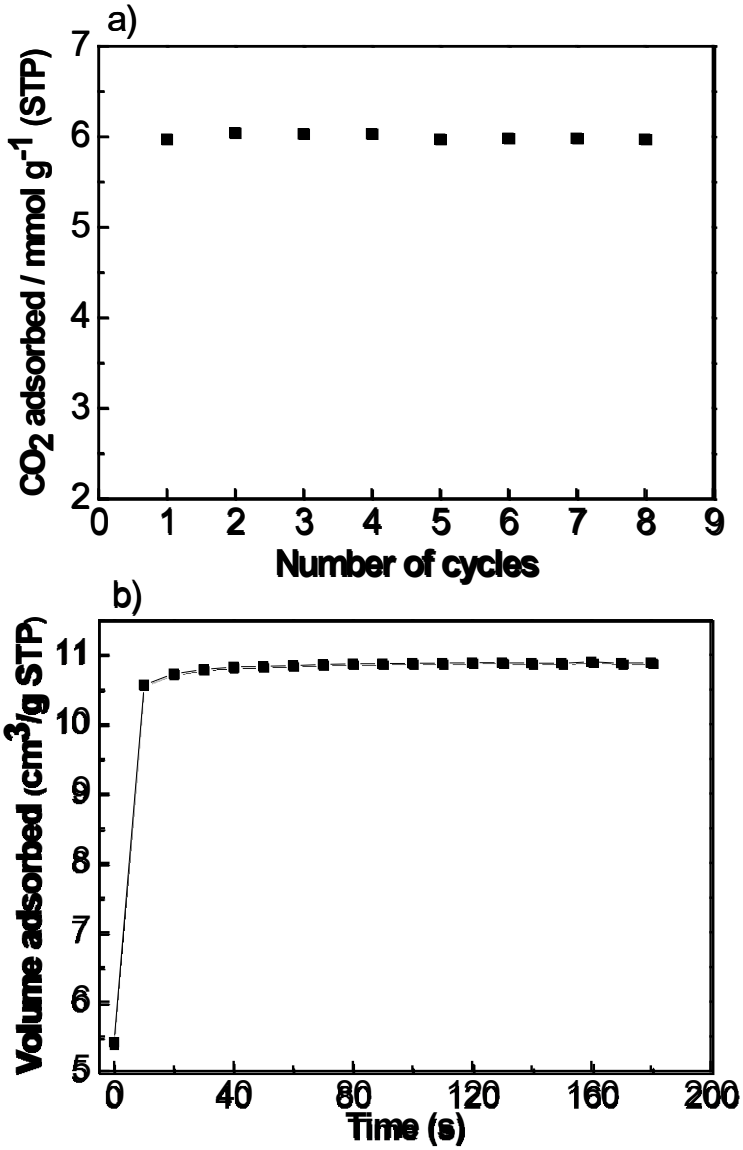

Figure 9. a) Cyclic CO_2 adsorption capacity of chemically activated carbon MAC-E-7 (activated at 700 °C from hydrothermally treated Eucalyptus lignin), recorded at 0 °C in pure CO_2 (eight cycles were performed and no high-temperature degassing was performed between runs); b) uptake kinetics for MAC-E-7, recorded at 0 °C by subjecting the sample to a small amount of pure CO_2.

The cycle time needs to be very short for adsorption-driven capture of CO_2. In relation to that, the adsorption and desorption times become important factors for tentative adsorption-driven processes for the capture of CO_2.[55,67] These times should be as small as possible. Hence, a good CO_2 sorbent should

have a fast adsorption and/or desorption rate. Figure 9b showed that MAC-E-7 could reach 95% of the CO_2 capacity within 10 s, which is fast and could be suitable for a sorbent used in a very rapid swing-sorption cycle of a CCS-based capture.

Using different hydrochars had a clear effect on the resulting MACs. This is likely due to the different composition and structure of the hydrochars. The hydrochars, in turn, are products of the origin of the lignin, i.e., the wood species, the process with which the lignin was liberated from the wood, i.e., the Kraft process or enzymatic hydrolysis, and the process parameters used in the lignin-to-liquid process.

Conclusions

The MACs were prepared from hydrochars, which is an example that waste products from lignin-to-liquid processes can be upgraded to potentially useful materials. The pore size distribution, surface area, and the ultramicropore volume could be varied by changing the temperature used for the chemical activation with KOH. When activated at a temperature of 700 °C, the MACs displayed very high ultramicropore volume and correspondingly a large uptake of CO2. These properties are important for the potential use of such sorbents as CO_2 sorbents; however, it appears that it would be beneficial to both the CO_2 capacity and CO_2-over-N_2 selectivity to further enhance the Q_{st} for CO_2 of the MACs. After being activated at 800 °C, the MACs displayed high specific surface areas and broad PSDs. Such properties are speculatively more relevant for uses in water purification or as supports for catalysis. The MACs contained significant amounts of embedded nanoparticles of iron with an iron oxide (magnetite) that displayed soft magnetic behavior with coercivities below 100 Oe.

Although out of the scope of this study, the magnetic properties of MACs may be used to facilitate the separation of PAC from liquids and have the potential to reduce desorption time, and therefore cycling time of CO_2 temperature swing processes through the application of electromagnetic fields. The potential catalytic properties of the MACs are also interesting, and some of these will be reported elsewhere.

AUTHOR INFORMATION

Corresponding Author

niklas.hedin@mmk.su.se

Present Addresses

Author Contributions

The manuscript was written through contributions of all authors. All authors have given approval to the final version of the manuscript. These authors contributed equally. (match statement to author names with a symbol)

Funding Sources

Notes

ACKNOWLEDGEMENT

This project was supported by the Swedish Energy Agency and by VR and VINNOVA. YT was supported by the Knut and Alice Wallenberg Foundation (Project: 3DEM-NATUR). GSA was supported by the Knut and Alice Wallenberg Foundation (3DEM-NATUR and Wallenberg Wood Science Center.

REFERENCES

(1) Shafiee, S.; Topal, E. When Will Fossil Fuel Reserves Be Diminished? Energy Policy 2009, 37 (1), 181−189.
(2) Höök, M.; Tang, X. Depletion of Fossil Fuels and Anthropogenic Climate Change-A Review. Energy Policy 2013, 52, 797−809.
(3) Zakzeski, J.; Bruijnincx, P. C. A.; Jongerius, A. L.; Weckhuysen, B. M. The Catalytic Valorization of Ligning for the Production of Renewable Chemicals. Chem. Rev. 2010, 110, 3552−3599.
(4) Azadi, P.; Inderwildi, O. R.; Farnood, R.; King, D. A. Liquid Fuels, Hydrogen and Chemicals from Lignin: A Critical Review. Renewable Sustainable Energy Rev. 2013, 21, 506−523.

(5) Kleinert, M.; Barth, T. Towards a Lignincellulosic Biorefinery: Direct One-Step Conversion of Lignin to Hydrogen-Enriched Biofuel. Energy Fuels 2008, 22 (2), 1371−1379.
(6) Pandey, M. P.; Kim, C. S. Lignin Depolymerization and Conversion: A Review of Thermochemical Methods. Chem. Eng. Technol. 2011, 34 (1), 29−41.
(7) Gosselink, R. J. A.; de Jong, E.; Guran, B.; Abächerli, A. Co- Ordination Network for Lignin - Standardisation, Production and Applications Adapted to Market Requirements (EUROLIGNIN). Ind. Crops Prod. 2004, 20 (2), 121−129.
(8) Guerra, A.; Filpponen, I.; Lucia, L. A.; Argyropoulos, D. S. Comparative Evaluation of Three Lignin Isolation Protocols for Various Wood Species. J. Agric. Food Chem. 2006, 54 (26), 9696−9705.
(9) Oregui Bengoechea, M.; Hertzberg, A.; Miletić, N.; Arias, P. L.; Barth, T. Simultaneous Catalytic de-Polymerization and Hydrodeoxygenation of Lignin in Water/formic Acid Media with Rh/Al2O3, Ru/Al2O3 and Pd/Al2O3 as Bifunctional Catalysts. J. Anal. Appl. Pyrolysis 2015, 113, 713−722.
(10) Bansal, R. C.; Goyal, M. Activated Carbon Adsorption; CRC Press, 2005.
(11) Ahmadpour, A.; Do, D. D. The Preparation of Active Carbons from Coal by Chemical and Physical Activation. Carbon 1996, 34 (4), 471−479.
(12) Prahas, D.; Kartika, Y.; Indraswati, N.; Ismadji, S. Activated Carbon from Jackfruit Peel Waste by H3PO4 Chemical Activation: Pore Structure and Surface Chemistry Characterization. Chem. Eng. J. 2008, 140 (1−3), 32−42.
(13) Schröder, E.; Thomauske, K.; Weber, C.; Hornung, A.; Tumiatti, V. Experiments on the Generation of Activated Carbon from Biomass. J. Anal. Appl. Pyrolysis 2007, 79 (1−2), 106−111.
(14) Alslaibi, T. M.; Abustan, I.; Ahmad, M. A.; Foul, A. A. A Review: Production of Activated Carbon from Agricultural Byproducts via Conventional and Microwave Heating. J. Chem. Technol. Biotechnol. 2013, 88 (7), 1183−1190.
(15) Suhas; Carrott, P. J. M.; Ribeiro Carrott, M. M. L. Lignin – from Natural Adsorbent to Activated Carbon: A Review. Bioresour. Technol. 2007, 98 (12), 2301−2312.
(16) Rodríguez-Mirasol, J.; Cordero, T.; Rodríguez, J. J. Preparation and Characterization of Activated Carbons from Eucalyptus Kraft Lignin. Carbon 1993, 31 (1), 87−95.
(17) Hayashi, J.; Kazehaya, A.; Muroyama, K.; Watkinson, A. P. Preparation of Activated Carbon from Lignin by Chemical Activation. Carbon 2000, 38 (13), 1873−1878.
(18) Sangchoom, W.; Mokaya, R. Valorization of Lignin Waste: Carbons from Hydrothermal Carbonization of Renewable Lignin as Superior Sorbents for CO2 and Hydrogen Storage. ACS Sustainable Chem. Eng. 2015, 3, 1658−1667.

(19) Balahmar, N.; Mitchell, A. C.; Mokaya, R. Generalized Mechanochemical Synthesis of Biomass-Derived Sustainable Carbons for High Performance CO2 Storage. Adv. Energy Mater. 2015, 5, 1500867.
(20) China Activated Carbon Industry Report, 2014-2017.
(21) Global Activated Carbon Market: 2014-2019.
(22) Activated Carbon Market Size, Price, Analysis Report, 2020.
(23) Carruthers, J. D.; Petruska, M. A.; Sturm, E. A.; Wilson, S. M. Molecular Sieve Carbons for CO2 Capture. Microporous Mesoporous Mater. 2012, 154, 62−67.
(24) Hao, G.-P.; Li, W.-C.; Qian, D.; Lu, A.-H. Rapid Synthesis of Nitrogen-Doped Porous Carbon Monolith for CO2 Capture. Adv. Mater. 2010, 22 (7), 853−857.
(25) Drage, T. C.; Blackman, J. M.; Pevida, C.; Snape, C. E. Evaluation of Activated Carbon Adsorption for CO2 Capture in Gasification. Energy Fuels 2009, 23 (14), 2790−2796.
(26) Plaza, M. G.; Pevida, C.; Martín, C. F.; Fermoso, J.; Pis, J. J.; Rubiera, F. Developing Almond Shell-Derived Activated Carbons as CO2 Adsorbents. Sep. Purif. Technol. 2010, 71 (1), 102−106.
(27) Presser, V.; McDonough, J.; Yeon, S.-H.; Gogotsi, Y. Effect of Pore Size on Carbon Dioxide Sorption by Carbide Derived Carbon. Energy Environ. Sci. 2011, 4 (8), 3059.
(28) Gibson, J. A. A.; Mangano, E.; Shiko, E.; Greenaway, A. G.; Gromov, A. V.; Lozinska, M. M.; Friedrich, D.; Campbell, E. E. B.; Wright, P. A.; Brandani, S. Adsorption Materials and Processes for Carbon Capture from Gas-Fired Power Plants: AMPGas. Ind. Eng. Chem. Res. 2016, 55 (13), 3840−3851.
(29) Zouboulis, A. I.; Lazaridis, N. K.; Zamboulis, D. Powdered Activated Carbon Separation from Water by Foam Flotation. Sep. Sci. Technol. 1994, 29 (3), 385−400.
(30) Tsukamoto, K. US Patent 4,260,523 A. 1979.
(31) Zhang, G.; Qu, J.; Liu, H.; Cooper, A. T.; Wu, R. CuFe2O4/activated Carbon Composite: A Novel Magnetic Adsorbent for the Removal of Acid Orange II and Catalytic Regeneration. Chemosphere 2007, 68 (6), 1058−1066.
(32) Qu, J. Research Progress of Novel Adsorption Processes in Water Purification: A Review. J. Environ. Sci. (Beijing, China) 2008, 20 (1), 1−13.
(33) Cazetta, A. L.; Pezoti, O.; Bedin, K. C.; Silva, T. L.; Paesano Junior, A.; Asefa, T.; Almeida, V. C. Magnetic Activated Carbon Derived from Biomass Waste by Concurrent Synthesis: Efficient Adsorbent for Toxic Dyes. ACS Sustainable Chem. Eng. 2016, 4 (3), 1058−1068.
(34) Šafařík, I.; Nymburská, K.; Šafaříková, M. Adsorption of Water- Soluble Organic Dyes on Magnetic Charcoal. J. Chem. Technol. Biotechnol. 1997, 69 (1), 1−4.

(35) Oliveira, L. C. A.; Rios, R. V. R. A.; Fabris, J. D.; Garg, V.; Sapag, K.; Lago, R. M. Activated Carbon/iron Oxide Magnetic Composites for the Adsorption of Contaminants in Water. Carbon 2002, 40 (12), 2177−2183.
(36) Hao, W.; Björkman, E.; Yun, Y.; Lilliestråle, M.; Hedin, N. Iron Oxide Nanoparticles Embedded in Activated Carbons Prepared from Hydrothermally Treated Waste Biomass. ChemSusChem 2014, 7 (3), 875−882.
(37) Hedin, N.; Lilliestråle, M.; Hao, W.; Björkman, E. WO 2014/027953A1, 2014.
(38) Rudge, S. R.; Kurtz, T. L.; Vessely, C. R.; Catterall, L. G.; Williamson, D. L. Preparation, Characterization, and Performance of Magnetic Iron-Carbon Composite Microparticles for Chemotherapy. Biomaterials 2000, 21 (14), 1411−1420.
(39) Wang, C.; Liu, Q.; Cheng, X.; Shen, Z. Adsorption and Desorption of Gold on the Magnetic Activated Carbon. J. Mater. Sci. Technol. 1994, 10 (2), 151−153.
(40) Gorria, P.; Sevilla, M.; Blanco, J. A.; Fuertes, A. B. Synthesis of Magnetically Separable Adsorbents through the Incorporation of Protected Nickel Nanoparticles in an Activated Carbon. Carbon 2006, 44 (10), 1954−1957.
(41) Akhtar, J.; Amin, N. A. S. A Review on Process Conditions for Optimum Bio-Oil Yield in Hydrothermal Liquefaction of Biomass. Renewable Sustainable Energy Rev. 2011, 15 (3), 1615−1624.
(42) Thompson, E.; Danks, A. E.; Bourgeois, L.; Schnepp, Z. Iron- Catalyzed Graphitization of Biomass. Green Chem. 2015, 17, 551−556.
(43) Sing, K. S. W.; Everett, D. H.; Haul, R. A. W.; Moscou, L.; Pierotti, R. A.; Rouquerol, J.; Siemieniewska, T. Reporting Physisorption Data for Gas/solid Systems with Special Reference to the Determination of Surface Area and Porosity. Pure Appl. Chem. 1985, 57 (4), 603−619.
(44) Raymundo-Pinero, E.; Kierzek, K.; Machnikowski, J.; Beguin, F. Relationship between the Nanoporous Texture of Activated Carbons and Their Capacitance Properties in Different Electrolytes. Carbon 2006, 44, 2498−2507.
(45) Sevilla, M.; Fuertes, A. B.; Mokaya, R. High Density Hydrogen Storage in Superactivated Carbons from Hydrothermally Carbonized Renewable Organic Materials. Energy Environ. Sci. 2011, 4, 1400−1410.
(46) Ding, L.; Zou, B.; Li, Y.; Liu, H.; Wang, Z.; Zhao, C.; Su, Y.; Guo, Y. The Production of Hydrochar-Based Hierarchical Porous Carbons for Use as Electrochemical Supercapacitor Electrode Materials. Colloids Surf., A 2013, 423, 104−111.
(47) Sevilla, M.; Fuertes, A. B. Sustainable Porous Carbons with a Superior Performance for CO2 Capture. Energy Environ. Sci. 2011, 4, 1765−1771.

(48) Wei, L.; Sevilla, M.; Fuertes, A. B.; Mokaya, R.; Yushin, G. Hydrothermal Carbonization of Abundant Renewable Natural Organic Chemicals for High-Performance Supercapacitor Electrodes. Adv. Energy Mater. 2011, 1, 356−361.
(49) Hao, W.; Björkman, E.; Lilliestråle, M.; Hedin, N. Activated Carbons Prepared from Hydrothermally Carbonized Waste Biomass Used as Adsorbents for CO2. Appl. Energy 2013, 112, 526−532.
(50) Hao, W.; Björkman, E.; Lilliestråle, M.; Hedin, N. Activated Carbons for Water Treatment Prepared by Phosphoric Acid Activation of Hydrothermally Treated Beer Waste. Ind. Eng. Chem. Res. 2014, 53, 15389−15397.
(51) Otowa, T.; Tanibata, R.; Itoh, M. Production and Adsorption Characteristics of MAXSORB: High-Surface-Area Active Carbon. Gas Sep. Purif. 1993, 7 (4), 241−245.
(52) Lee, Y.-C.; Lee, S. M.; Hong, W. G.; Huh, Y. S.; Park, S. Y.; Lee, S. C.; Lee, J.; Lee, J. B.; Lee, H. U.; Kim, H. J. Carbon Dioxide Capture on Primary Amine Groups Entrapped in Activated Carbon at Low Temperatures. J. Ind. Eng. Chem. 2015, 23, 16−20.
(53) Alabadi, A.; Razzaque, S.; Yang, Y.; Chen, S.; Tan, B. Highly Porous Activated Carbon Materials from Carbonized Biomass with High CO2 Capturing Capacity. Chem. Eng. J. 2015, 281, 606−612.
(54) Songolzadeh, M.; Soleimani, M.; Takht Ravanchi, M.; Songolzadeh, R. Carbon Dioxide Separation from Flue Gases: A Technological Review Emphasizing Reduction in Greenhouse Gas Emissions. Sci. World J. 2014, 2014, 1−34.
(55) Samanta, A.; Zhao, A.; Shimizu, G. K. H.; Sarkar, P.; Gupta, R. Post-Combustion CO2 Capture Using Solid Sorbents: A Review. Ind. Eng. Chem. Res. 2012, 51 (4), 1438−1463.
(56) Sevilla, M.; Falco, C.; Titirici, M.-M.; Fuertes, A. B. High- Performance CO2 Sorbents from Algae. RSC Adv. 2012, 2 (33), 12792−12797.
(57) Deng, S.; Wei, H.; Chen, T.; Wang, B.; Huang, J.; Yu, G. Superior CO2 Adsorption on Pine Nut Shell-Derived Activated Carbons and the Effective Micropores at Different Temperatures. Chem. Eng. J. 2014, 253, 46−54.
(58) Montagnaro, F.; Silvestre-Albero, A.; Silvestre-Albero, J.; Rodríguez-Reinoso, F.; Erto, A.; Lancia, A.; Balsamo, M. Post-Combustion CO2 Adsorption on Activated Carbons with Different Textural Properties. Microporous Mesoporous Mater. 2015, 209, 157− 164.
(59) Aaron, D.; Tsouris, C. Separation of CO2 from Flue Gas: A Review. Sep. Sci. Technol. 2005, 40 (1−3), 321−348.
(60) Myers, A. L.; Prausnitz, J. M. Thermodynamics of Mixed-Gas Adsorption. AIChE J. 1965, 11 (1), 121−127.

(61) Yi, H.; Li, F.; Ning, P.; Tang, X.; Peng, J.; Li, Y.; Deng, H. Adsorption Separation of CO2, CH4, and N2 on Microwave Activated Carbon. Chem. Eng. J. 2013, 215−216, 635−642.
(62) Belmabkhout, Y.; Sayari, A. Adsorption of CO2 from Dry Gases on MCM-41 Silica at Ambient Temperature and High Pressure. 2: Adsorption of CO2/N2, CO2/CH4 and CO2/H2 Binary Mixtures. Chem. Eng. Sci. 2009, 64, 3729−3735.
(63) Chue, K. T.; Kim, J. N.; Yoo, Y. J.; Cho, S. H.; Yang, R. T. Comparison of Activated Carbon and Zeolite 13X for CO2 Recovery from Flue Gas by Pressure Swing Adsorption. Ind. Eng. Chem. Res. 1995, 34 (2), 591−598.
(64) Guo, B.; Chang, L.; Xie, K. Adsorption of Carbon Dioxide on Activated Carbon. J. Nat. Gas Chem. 2006, 15, 223−229.
(65) Yu, L.; Falco, C.; Weber, J.; White, R. J.; Howe, J. Y.; Titirici, M.-M. Carbohydrate-Derived Hydrothermal Carbons: A Thorough Characterization Study. Langmuir 2012, 28 (33), 12373−12383.
(66) González, A. S.; Plaza, M. G.; Rubiera, F.; Pevida, C. Sustainable Biomass-Based Carbon Adsorbents for Post-Combustion CO2 Capture. Chem. Eng. J. 2013, 230, 456−465.
(67) Hedin, N.; Andersson, L.; Bergström, L.; Yan, J. Adsorbents for the Post-Combustion Capture of CO2 Using Rapid Temperature Swing or Vacuum Swing Adsorption. Appl. Energy 2013, 104, 418−433.
(68) Dunne, J. A.; Mariwala, R.; Rao, M.; Sircar, S.; Gorte, R. J.; Myers, A. L. Calorimetric Heats of Adsorption and Adsorption Isotherms. 1. O2, N2, Ar, CO2, CH4, C2H6, and SF6 on Silicalite. Langmuir 1996, 12 (3), 5888−5895.
(69) Couck, S.; Denayer, J. F. M.; Baron, G. V.; Remy, T.; Gascon, J.; Kapteijn, F. An Amine-Functionalized MIL-53 Metal – Organic Framework with Large Separation Power for CO2 and CH4. J. Am. Chem. Soc. 2009, 131, 6326−6327.
(70) Huang, Y.-Y. The Temperature Dependence of Isosteric Heat of Adsorption on the Heterogeneous Surface. J. Catal. 1972, 25, 131−138.